Check for updates

194426, 2022, 7, Dowlondoed from https://onlinelibrary.wiley.com/doi/10.1002/ente.202200251 by Forschung.szentrum Jülich GmbH Research Center, Wiley Online Library on [11/11/2022]. See the Terms and Conditions (https://onlinelibrary.wiley.com/terms-and-conditions) on Wiley Online Library for rules of use; O. Articles as governed by the applicable Creative Commons Licenses

Closed-Loop Adsorption-Based Upgrading of Heat from 90 to 110 °C: Experimental Demonstration and Insights for Future Development

Mirko Engelpracht,* Jannik Driesel, Oliver Nießen, Matthias Henninger, Jan Seiler, and André Bardow*

Industrial energy efficiency can be increased by recovering waste heat, mainly available below 100 °C. This low-temperature waste heat can drive adsorption heat transformers (AdHTs) to upgrade waste heat to industrially relevant temperatures above 100 °C. Flexible process integration can be achieved by decoupling adsorptive and heat transfer fluid in closed-loop cycles. However, the experimental feasibility of closed-loop AdHTs has not been shown yet. Hence, this work studies an experimental one-bed setup of an AdHT based on a closed-loop cycle using silica gel 123 and water as the working pair. Experimental feasibility is demonstrated for heat transformation from 90 to 110 °C with waste heat released at 25 °C. The highest coefficient of performance (COP) is 0.183 J J⁻¹ (23% of the maximum Carnot efficiency), and the highest specific heating power (SHP) is 168 W kg⁻¹. A systematic variation of the operating conditions shows that efficiency COP and power density SHP strongly depend on the operating temperatures, volume flows, and phase times. Furthermore, avoiding condensation inside the adsorber casing and heat losses are identified to be crucial for the design of AdHTs. In summary, AdHTs based on a closed-loop cycle show a promising performance to recover low-temperature waste heat.

M. Engelpracht, J. Driesel, O. Nießen, M. Henninger Chair of Technical Thermodynamics Faculty of Mechanical Engineering RWTH Aachen University Schinkelstraße 8, 52062 Aachen, Germany E-mail: mirko.engelpracht@ltt.rwth-aachen.de

I. Seiler, A. Bardow Energy & Process Systems Engineering Department of Mechanical and Process Engineering ETH Zurich Tannenstrasse 3, 8092 Zürich, Switzerland

E-mail: abardow@ethz.ch

Institute of Energy and Climate Research - Energy Systems Engineering (IEK-10) Forschungszentrum Jülich GmbH Wilhelm-Johnen-Straße, 52425 Jülich, Germany

The ORCID identification number(s) for the author(s) of this article can be found under https://doi.org/10.1002/ente.202200251.

© 2022 The Authors. Energy Technology published by Wiley-VCH GmbH. This is an open access article under the terms of the Creative Commons Attribution-NonCommercial License, which permits use, distribution and reproduction in any medium, provided the original work is properly cited and is not used for commercial purposes.

DOI: 10.1002/ente.202200251

1. Introduction

Members of the United Nations strive to achieve a sustainable future by defining Sustainable Development Goals (SDGs) and accepting the Paris Climate Agreement.[1] For reaching the interdependent SDGs, six profound transformations have been proposed, with the third transformation aiming at "energy decarbonization and sustainable industry."[2] One measure for a sustainable industry is to increase industrial energy efficiency, [2,3] e.g., by utilization of waste heat, [3,4] which is mainly available below 100 °C. [5] Utilization of this low-temperature waste heat often requires heat transformation: e.g., 70-88% of the European heat demand is required above 100 °C^[6-8] with about 11% already occurring between 100 and 150 °C. [6] The overall heat demand causes about 64% of the European industrial final

energy consumption.^[7] Thus, the transformation of low-temperature waste heat to temperatures above 100 °C promises to reduce industrial primary energy consumption.

For transforming heat, the literature has recently discussed thermally driven heat transformers based on thermochemical reactions^[9] or absorption^[10] and adsorption^[11,12] phenomena. A comparison of these heat transformers was performed in our previous article. [13] Among these three heat transformers, adsorption heat transformers (AdHTs) are particularly promising as they are often based on weak physical interactions, allowing very low-temperature waste heat below 60 °C as driving energy. [14] Besides, AdHTs can employ nontoxic working pairs with high material stabilities and working capacities (e.g., AQSOA zeolites and water),^[15] which are already well known from adsorption chillers.^[15,16] Thus, AdHTs are an environmentally friendly technology that could increase energy efficiency, leading to a more sustainable industry.

AdHTs use either an open- or a closed-loop cycle: open-loop cycles exploit direct contact of the liquid adsorptive and the solid adsorbent for generating steam with temperatures above 100 °C and have been studied in the literature extensively.[17-22] For example, researchers have demonstrated the experimental feasibility of cyclic steam generation using zeolite 13X and water as the working pair, [17,18] and developed and validated a dynamic

2194965, 2022, 7, Downloaded from https://onlinelibrary.wiley.com/doi/10.1002/ente.202200251 by Forschungszentrun Jülich GmbH Research Center, Wiley Online Library on [11/11/2021], See the Terms and Conditions (https://onlinelibrary.wiley.com/com/onlinelibrary.wiley.com/com/onlinelibrary.on/onlinelibrary.wiley.com/com/onlinelibrary.wile

model to support improvements in the system performance. [19] Moreover, it has been experimentally shown that composite zeolites $^{[20,21]}$ or heat and mass recovery $^{[22]}$ increase the system performance, such as temperature lift, generated steam mass, or efficiency. However, open-loop cycles might be challenging to integrate into industrial processes as the adsorptive is also the heat transfer fluid. Adsorptive and heat transfer fluid are decoupled in closed-loop cycles.

Closed-loop cycles have been studied mainly for the utilization of ambient heat at temperatures around 0 °C to generate useful heat at domestically relevant temperatures such as 30-40 °C. [12,23] Aristov and co-workers have comprehensively studied the optimal working pair both theoretically and experimentally to increase useful heat generation and, thus, the cycle performance. [24] Important progress has been made, e.g., the theoretical derivation showing that the optimal working pair requires a convex/concave sorption isotherm for adsorption/desorption^[25] or the experimental demonstration of pressure-initiated desorption at very low vapor pressures. [26] Moreover, different prototypes of closed-loop cycles have been studied experimentally at low temperatures, finding the following: 1) the cycle is experimentally feasible with a one-bed prototype and ACM35.4 and methanol as working pair, [27] 2) composite adsorbents generate more useful heat than conventional adsorbents for the studied operating conditions, [28] and 3) a two-bed prototype can generate useful heat quasicontinuously. [29]

In contrast, closed-loop cycles have been rarely studied for heat transformation around 100 °C to recover industrial low-temperature waste heat. Two theoretical studies determined the maximal performance from a thermodynamic perspective using idealized steady-state models. [11,14] Particularly, these models allow to screen for suitable working pairs depending on the operating temperatures, [14] with promising examples in these studies as well.^[14] Besides, these studies found the following: 1) working pairs with S-shaped isotherms are advantageous for achieving high efficiencies, [11] 2) new-generation composite adsorbents increase working capacity and efficiency compared to pure adsorbents, [14] 3) an assumed pinch temperature of 5 K within the heat exchangers can more than halve the achievable efficiency, [11,14] and 4) heat recovery in a two-bed cycle can increase the achievable efficiency up to 50%. [11,14] To also account for adsorption kinetics and thermal masses, we recently developed a dynamic model of a one-bed cycle assuming an ideal evaporator and condenser. [13] We simultaneously optimized the adsorber heat exchanger design and cycle control to evaluate the AdHT performance: for the working pair AQSOA Z02 and water, we determined exergy efficiencies greater than 60% with power densities higher than 600 W kg⁻¹ when transforming heat from 90 to 110 °C and releasing heat of condensation at 35 °C. [13] Thus, AdHTs based on a closed-loop cycle seem promising for transforming low-temperature waste heat to industrially relevant temperatures above 100 °C.

However, to the best of the authors' knowledge, the experimental feasibility of an AdHT based on a closed-loop cycle has not been demonstrated for heat transformation around 100 °C. Therefore, in this work, we designed and built a lab-scale, onebed AdHT based on a closed-loop cycle, allowing us to assess the AdHT performance systematically. Section 2 describes the working principle of a closed-loop, one-bed AdHT and the experimental setup, key performance indicators, and operating conditions investigated in this work. In Section 3, we present the experimental results of one AdHT cycle in full detail and analyze the impacts of various operating conditions on the AdHT performance. Finally, Section 4 summarizes the main conclusions.

2. Experimental Section

First, we introduce the working principle of an ideal, one-bed AdHT based on a closed-loop cycle in Section 2.1. Then, we describe the experimental setup (Section 2.2), experimental procedure (Section 2.3), and key performance indicators (Section 2.4) used to evaluate the AdHT performance. Finally, we present the operating conditions investigated in this work in Section 2.5.

2.1. Working Principle

An AdHT based on a closed-loop cycle generates useful heat at a high temperature T_{high} by using heat at a medium temperature $T_{\rm med}$ as driving energy and rejecting waste heat at a low temperature T_{low} . The temperature difference between the medium and low temperature T_{med} – T_{low} is the so-called temperature thrust (TT), while the temperature difference between the high and medium temperature T_{high} – T_{med} is the so-called temperature lift (TL).^[30]

A simple implementation of the AdHT is a one-bed cycle, consisting of the three heat exchangers such as condenser, evaporator, and adsorber.^[11] Additionally, a small pump returns condensed adsorptive from the condenser into the evaporator.^[11] The ideal, one-bed AdHT cycle is a pressure-driven, cyclic batch process that consists of four main phases, already described in full detail in the literature.[11,13,31] Nevertheless, we briefly describe the main phases using an isosteric diagram (cf., Figure 1a), allowing us to describe the experimental setup and procedure more clearly in Section 2.2 and 2.3.

The first phase is adsorption-based heating (1-2, cf., Figure 1a), in which the regenerated adsorber (i.e., state 1) is heated to the high temperature T_{high} by the heat of adsorption released while adsorbing. For this purpose, the heat transfer fluid of the adsorber flows through a bypass (cf., Figure 1b), thus decoupling the adsorber from its secondary heat circuit. Adsorption occurs because vaporous adsorptive flows from the evaporator into the adsorber (cf., Figure 1b) due to a pressure difference. In the evaporator, the supplied heat flow Q_{evap} continuously vaporizes liquid adsorptive at constant medium temperature $T_{\rm med}$ and thus constant vapor pressure $p_{\rm med}^{\rm sat}$ (cf., Figure 1a). Once the adsorber reaches the high temperature T_{high} , the adsorption-based heating ends.

The second phase generates a useful heat flow \dot{Q}_{use} at the high temperature T_{high} by further releasing the heat of adsorption: the useful heat flow $Q_{\rm use}$ is released isothermally in the ideal case (2–3, cf., Figure 1a),^[11] while nonconstant temperatures higher than T_{high} occur in practice (2–2*–3, cf., Figure 1a).^[31] For extracting the useful heat flow \dot{Q}_{use} , the heat transfer fluid of the adsorber now flows through the adsorber (cf., Figure 1c). Thereby, the inlet temperature of the heat transfer fluid defines the use cases of the AdHT, which are described in more detail below. The use phase ends once the adsorber pressure reaches

21944296, 2022, 7, Downloaded from https://onlinelibrary.wiley.

and-conditions) on Wiley Online Library for rules of use; OA articles are governed by the applicable Creative Commons

www.advancedsciencenews.com

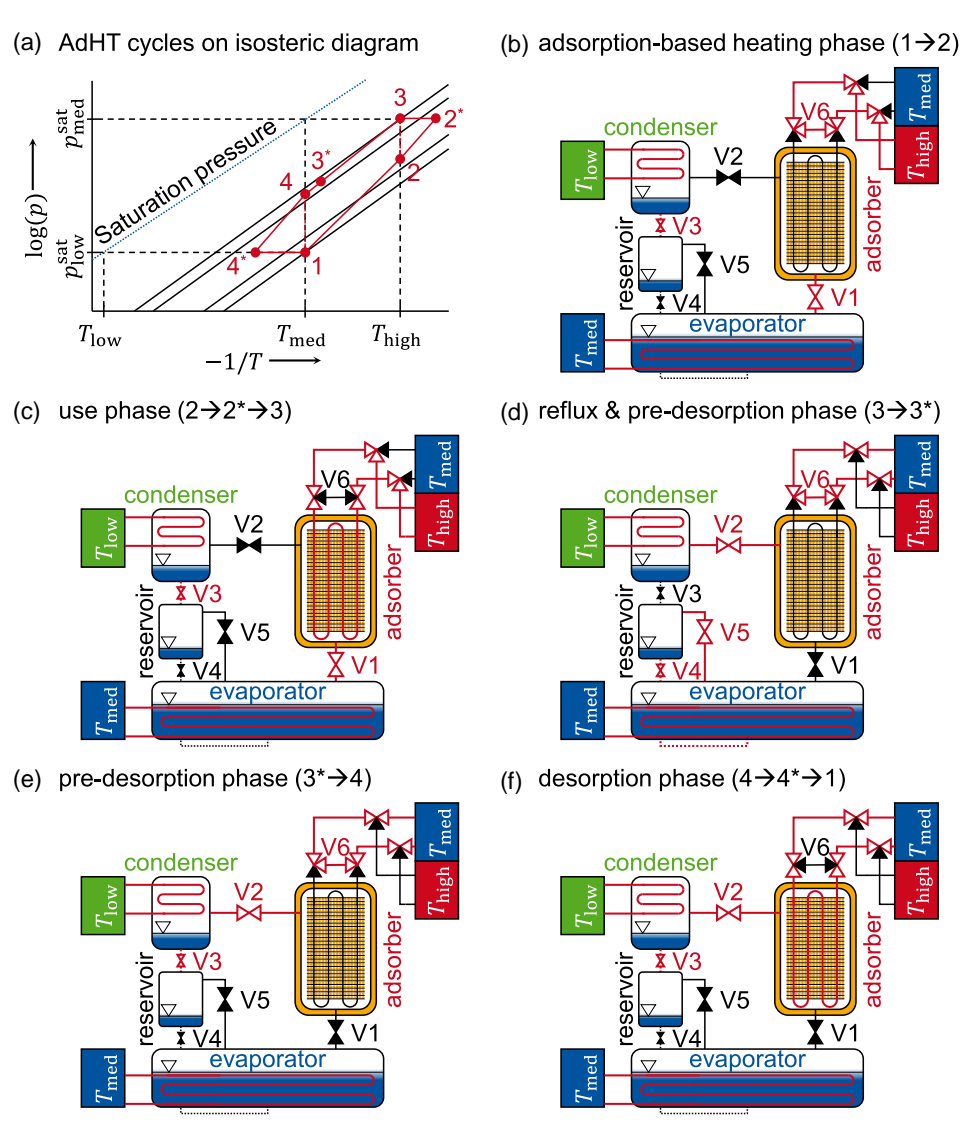


Figure 1. a) Phases of a one-bed adsorption heat transformer cycle (ideal: 1-2-3-4-1; nonideal: $1-2-2^*-3-3^*-4-4^*-1$) working at the temperature triple $T_{\text{low}}/T_{\text{med}}/T_{\text{high}}$ and saturation vapor pressures $p_{\text{low}}^{\text{sat}}/p_{\text{med}}^{\text{sat}}$ shown in an isosteric diagram. Implementation of the cycle phases in the experimental setup: b) adsorption-based heating phase (1-2), c) use phase (2-2*-3), d) reflux and predesorption phase (3-3*), e) predesorption phase (3*-4), and (f) desorption phase (4-4*-1). Red thick lines indicate secondary circuits or internal steam/liquid pipes that are active, and color-filled valves are closed.

the vapor pressure at medium temperature $p_{\rm med}^{\rm sat}$ and the adsorber temperature reaches the high temperature $T_{\rm high}$.

The third phase is predesorption (3–3*–4, cf., Figure 1a), in which the loaded adsorber (i.e., state 3) is cooled from the high temperature $T_{\rm high}$ to the medium temperature $T_{\rm med}$. The heat transfer fluid of the adsorber flows again through the bypass (cf., Figure 1e), thus decoupling the adsorber from its secondary heat circuit again. Due to a pressure difference, desorbed vaporous adsorptive flows from the adsorber into the condenser (cf., Figure 1e). The required heat of desorption is provided by the sensible heat of the adsorber itself, which thereby cools down. In the condenser, the heat flow $\dot{Q}_{\rm cond}$ is released to the environment allowing continuous condensation of the adsorptive at constant vapor pressure $p_{\rm low}^{\rm sat}$ and constant low temperature

 T_{low} (cf., Figure 1a). Once the adsorber reaches the medium temperature T_{med} , the predesorption ends.

The last phase continues the desorption. A desorption heat flow $Q_{\rm des}$ is absorbed isothermally at the medium temperature $T_{\rm med}$ in the ideal case (4–1, cf., Figure 1a), [11] while the temperature reduces below $T_{\rm med}$ in practice (4–4*–1, cf., Figure 1a). For providing the desorption heat flow $Q_{\rm des}$, the heat transfer fluid of the absorber flows again through the adsorber (cf., Figure 1f). The desorption phase ends once the adsorber pressure reaches the vapor pressure at low temperature $p_{\rm low}^{\rm sat}$ and the adsorber temperature reaches the medium temperature $T_{\rm med}$.

For closing the AdHT cycle, a small pump returns the condensed adsorptive from the condenser into the evaporator during

21944296, 2022, 7, Downloaded from https://onlinelibrary.wiley.com/doi/10.1002/ente.202200251 by Forschungs

Jülich GmbH Research Center, Wiley Online Library on [11/11/2022]. See the Terms and Conditions (https://onlinelibrary.wiley.com/terms

and-conditions) on Wiley Online Library for rules of use; OA articles are governed by the applicable Creative Commons I

all desorption phases (i.e., predesorption and desorption). Note that we realized the condensate reflux without a pump in this work and, therefore, no pump is shown in Figure 1. Instead, we returned the condensate during the reflux and predesorption phase (3–3*, cf., Figure 1d) by exploiting gravity and the pressure difference between condensate reservoir and evaporator. More details of the experimental procedure are given in Section 2.3.

The AdHT cycle described above can be applied for two use cases that only differ in the inlet temperature of the adsorber's heat transfer fluid during the use phase. 1) For the use case "constant temperature," the inlet temperature of the adsorber's heat transfer fluid is T_{high} , representing, e.g., steam generation at a constant temperature. 2) In the use case "temperature lift," the adsorber's heat transfer fluid increases its temperature from $T_{
m med}$ at the inlet of the adsorber to at least $T_{
m high}$ at the outlet of the adsorber. This use case represents a classical heat-pump application in heating networks. Thus, the phases of the AdHT cycle are the same, except for the two thermostats of the adsorber that are both operated at the medium temperature $T_{\rm med}$ for the use case "temperature lift" while one is operated at the medium temperature $T_{\rm med}$ and the other at the high temperature $T_{\rm high}$ for the use case "constant temperature." The use case "constant temperature" has been predominantly studied in the literature. However, the use case "temperature lift" might be more universally applicable in industrial processes. Hence, we assess the performance of both use cases in this work.

2.2. Experimental Setup

The experimental setup (cf., Figure 2) was built to systematically assess the performance of a one-bed AdHT based on a closedloop cycle (cf., Figure 1) at different operating conditions such as operating temperatures or phase times. For this purpose, the control of the experimental setup was entirely automated using a control system written in LabVIEW 2017, allowing a simple reproduction of experiments.

The main components of the AdHT are the three heat exchangers condenser, evaporator, and adsorber within vacuumtight, cylindric, stainless steel casings (Table 1). The evaporator and adsorber casings are modular in design using ISO-K flanges, allowing the heat exchangers to be replaced quickly. Water is the heat transfer fluid in all three heat exchangers: the water is at ambient pressure in the condenser and evaporator, while it is pressurized to 10 bar in the adsorber. The high pressure in the adsorber is prescribed by safety reasons of the existing hydraulic adsorber circuit as the circuit also allows for higher temperatures than investigated in this work. The water temperatures are kept constant at the heat exchanger inlets by using thermostats (Figure 2a and Table 2): one thermostat for the condenser and evaporator each, and two thermostats for the adsorber. The two thermostats of the adsorber allow changing the water temperature between the medium temperature $T_{\rm med}$ and high temperature $T_{\rm high}$ rapidly.^[32]

In addition to the three heat exchangers, another important component is a vacuum-tight, rectangular, stainless steel reservoir (casing mass: 4.8 kg, liquid adsorptive capacity: 1 L) to store condensed adsorptive between the condenser and evaporator. ISO-KF-flanges and ISO-KF pipes connect all components: the

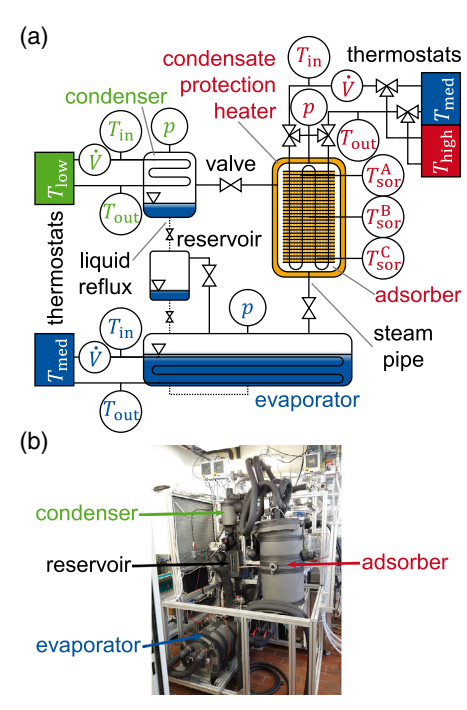


Figure 2. a) Scheme of the experimental setup. Circles indicate measurement sensors: p-pressure transducer, T-temperature sensor, and V—volume flow sensor. Indices indicate positions of measurement sensors: in-inlet, out-outlet, and sor-adsorbent. Solid connections of main components indicate steam pipes, and dotted connections indicate liquid pipes. b) Photograph of the lab-scale adsorption heat transformer.

pipes for steam (inner diameter: 40 mm) can be cut off by pneumatically operated butterfly valves, while solenoid valves can cut off the pipes for liquids (inner diameter: 16 mm). All pipes and other components are thermally insulated to avoid heat losses between the components and the environment.

The working pair selected was silica gel 123 and water based on an internal preliminary steady-state analysis and good availability. The adsorbent was produced by W. R. Grace & Co. and had a spherical granular shape with an average diameter of $0.9 \, \text{mm}$ and a bulk density of about $710 \, \text{kg m}^{-3}$. In total, 1.9 kg of dry granular adsorbent was filled in the void between the fins of the adsorber heat exchanger. The adsorber has a condensate protection heater that can be optionally operated to avoid the condensation of vaporous adsorptive on the inner surface of the adsorber casing. For this purpose, a hose made from rubber (length: $60 \,\mathrm{m}$, diameter: $\varnothing 12 \times 2.5 \,\mathrm{mm}$) is completely wrapped around the cylindrical adsorber casing. The heat transfer fluid is again water, with its inlet temperature kept constant by an additional thermostat (Table 2).

For evaluating the AdHT performance, measurement sensors are installed in the secondary circuits of each heat exchanger (Figure 2a). Temperature and volume flow sensors are placed at the inlets, while only temperature sensors are installed at the outlets. Moreover, pressure transducers are placed at the evaporator, condenser, and adsorber, and three additional temperature sensors measure the adsorbent temperature within the adsorber heat exchanger. All temperature sensors were

21944296, 2022, 7, Downloaded from https://onlinelibrary.wiley.com/doi/10.1002/ente.202200251 by Forschungszentrum

Jülich GmbH Research Center, Wiley Online Library on [11/11/2022]. See the Terms

nditions) on Wiley Online Library for rules of use; OA articles are governed by the applicable Creative Commons License

Table 1. Geometric details and further specifications of the main components of the AdHT prototype.

Description	Unit Condenser		Evaporator	Absorber		
Casing						
Dimensions	mm	Length: 220	Length 836	Length: 650		
		Diameter: Ø120 \times 2.5	Diameter: Ø324 $ imes$ 3	Diameter Ø324 $ imes$ 3		
Metal mass	kg	2.7	58.9	50.9		
Heat exchanger						
Dimensions	mm	Double helix made	14 identical, capillary active copper tubes	Finned-tube heat exchanger made from copper		
		from copper tube	covered with circular fins and connected	with rectangular fins and two layers of five tubes		
		Length: 3984	serially in a single layer ^[33]	each, all connected serially		
		Diameter: Ø10 \times 1	Length: 7208	Length: 4100		
			Diameter: Ø17 \times 0.7	Diameter: \emptyset 12 \times 0.32		
			Fin height: 0.9	Fin height: 32		
			Fin thickness: 0.3	Fin width: 27.7		
			Fin pitch: 0.64	Fin thickness: 0.12		
				Fin pitch: 2		
Area at heat transfer fluid side	m^2	0.10	0.34	0.15		
Area at adsorptive/adsorbent side	m^2	0.13	1.24	3.43		
Metal mass	kg	1.2	4.3	5.0		
Heat transfer fluid mass	kg	0.2	1.3	0.4		
Liquid adsorptive mass	kg	0.5	29.5	_		

Table 2. Specifications of measurement equipment and thermostats, with locations given in Figure 2a. All uncertainties are given for a standard uncertainty (i.e., coverage factor k = 1), and the uncertainty of temperature sensors is the upper limit after applying the calibration procedures (cf., Section A, Supporting Information).

Measurement sensors					
Sensors	Manufacturer	Model	Unit	Uncertainty	
Pressure	Keller AG für Druckmesstechnik	PAA-33X, 1 bar, digitally read	mbar	±1	
Temperature	SE Sensor Electric	Pt100 type, class A, four-wire connection	K	±0.06	
Volume flow	Endress+Hauser AG	5P5B15-4VT7/0 and 5P5B25-6HL0/0, both models digitally read	L min ⁻¹	$\pm 0.5\%$ of measured value	
Thermostats					
Location	Manufacturer	Model	Unit	Temperature stability	
Condenser and evaporator	Peter Huber Kältemaschinenbau AG	CC-510w with Pilot ONE	K	± 0.02	
Adsorber: Medium temperature	Single Temperiertechnik GmbH	Compact TKS-90-9-116	К	±1	
Adsorber: High temperature	Single Temperiertechnik GmbH	Advanced NS-180-24-65	К	±1	
Adsorber: Condensate protection	Thermo Fisher Scientific Inc.	N6-C41	K	±0.1	

calibrated using two high-accuracy temperature sensors (Ahlborn, PT100 type FPA923L0250 read with data logger Ahlborn, ALMEMO 1030-2) to increase measurement accuracy (cf., Section A, Supporting Information). Table 2 summarizes the measurement uncertainties of all sensors and further specifications.

2.3. Experimental Procedure

Before starting the automated measurement campaigns, the experimental setup was prepared in four steps. First, the entire experimental setup was heated to the maximum achievable temperatures of the components (condenser: 75 °C, evaporator: 90 °C, adsorber: 160 °C) and evacuated for 12 h. All valves were opened permanently (cf., Figure 2a), and neither adsorptive nor adsorbent was inside the experimental setup. Second, a leakage test was performed using a quasi-isothermally pressure rise test for 72 h, finding a pressure increase of 1.3 Pa h^{-1} . The calculated air leak rate results in 4.81×10^{-4} mbar L s⁻¹.[34] Thus, the experimental setup was considered sufficiently vacuum-tight for the conducted measurement campaigns, mainly because 1) infiltrated inert gas was quickly extracted via a vacuum pump

www.entechnol.de

between all measurements and 2) all measurements were shorter than 6–8 h. Third, the evaporator and condenser were filled with degassed water, and the adsorbent was filled between the fins of the adsorber heat exchanger. Fourth, the components were separated by closing all valves except the valve between the condenser and reservoir (cf., Figure 2a). The components were heated to the maximum achievable temperatures and evacuated again to remove inert gas, possibly infiltrating the experimental setup during step three.

After finishing the one-time preparation of the experimental setup, all measurement campaigns were performed automatically using the LabVIEW-based control program. Each measurement started with an initial heating phase in which all thermostats were set according to the operating temperatures and volume flows, and the main components were heated up until reaching quasi-steady-state conditions. Subsequently, the AdHT cycle was repeatedly measured until reaching a cyclic-steady-state condition, and 3–6 repeated AdHT cycles were recorded afterward.

The implementation of the AdHT cycle largely corresponded to the AdHT cycle described in Section 2.1. However, the condensate reflux was realized differently because no suitable condensate pump was available when performing the measurement campaigns. Instead, the condensate was gravitationally returned in an additional phase of the AdHT cycle (cf., Figure 1d) in three steps: 1) the reservoir was separated from the condenser, 2) the vapor phases of the reservoir and evaporator were connected for pressure equalization, and 3) the liquid phases of the reservoir and evaporator were connected for the actual condensate reflux. The condensate was returned by gravity as the reservoir was installed higher than the evaporator in the experimental setup (cf., Figure 2). The condensate reflux was performed simultaneously with predesorption (cf., Figure 1d), thus not unnecessarily increasing the overall cycle time.

2.4. Key Performance Indicators

To assess the AdHT performance, we used the two key performance indicators 1) coefficient of performance (COP) and 2) specific heating power (SHP), defined by

$$COP = \frac{\int_{\tau_{cycle,end}}^{\tau_{cycle,end}} \dot{Q}_{use} d\tau}{\int_{\tau_{cycle,estart}}^{\tau_{cycle,end}} \dot{Q}_{evap} d\tau + \int_{\tau_{cycle,start}}^{\tau_{cycle,end}} \dot{Q}_{des} d\tau} = \frac{Q_{use}}{Q_{evap} + Q_{des}}$$
(1)

$$SHP = \frac{\int_{\tau_{\text{cycle,end}}}^{\tau_{\text{cycle,end}}} \dot{Q}_{\text{use}} d\tau}{(\tau_{\text{cycle,end}} - \tau_{\text{cycle,start}}) m_{\text{sor}}}$$
(2)

The COP relates the useful heat $Q_{\rm use}$ to the heat amounts required for vaporization $Q_{\rm evap}$ and desorption $Q_{\rm des}$. The three heat amounts are calculated by integrating the corresponding heat flows $Q_{\rm use}$, $Q_{\rm evap}$, and $Q_{\rm des}$ from cycle start $\tau_{\rm cycle,start}$ to cycle end $\tau_{\rm cycle,end}$. The COP describes the energy efficiency (i.e., first-law efficiency) of the AdHT. In contrast, the SHP relates the average useful heat flow over one cycle to the dry adsorbent mass $m_{\rm sor}$, thus considering system dynamics and system size. Note that a volumetric heating power could be used instead of the SHP for systems limited in size. The SHP values given can

be easily converted by multiplying by the dry sorbent mass (i.e., 1.9 kg, cf., Section 2.2) and then dividing by the desired reference volume, e.g., the volumes of the main components (cf., Table 1) or the volume of the adsorber heat exchanger (i.e., 6.3 L). The heating power normalized by the adsorber heat exchanger can thus be determined by multiplying the SHP with 0.30 kg $\rm L^{-1}$ (= $1.9\,\rm kg\,6.3^{-1}\,L^{-1}$). Both key performance indicators have a trade-off: the COP becomes maximal at longer cycle times because the actual AdHT cycle approaches the ideal AdHT cycle, whereas the SHP has a maximum at shorter cycle times. $\rm ^{[13]}$

Note that the condensate protection heater around the adsorber casing (cf., Figure 2a) should be theoretically included as an additional expense in Equation (1) as it inserts an additional heat flow into the adsorber. However, we neglect this heat flow for four reasons: first, condensation on the inner surface of the adsorber casing is avoidable when redesigning the adsorber heat exchanger. The vaporous adsorptive would not be in direct contact with the casing if the vaporous adsorptive flowed from the adsorber center to the adsorbent instead of from the adsorber outside. For this purpose, the arrangement of the adsorber heat exchanger would have to be changed from "casing-vaporous adsorptive-adsorbent-heat transfer fluid" to "casing-heat transfer fluid—adsorbent—vaporous adsorptive." Thus, condensation would be avoided, and a condensation protection heater would not be necessary. Second, the condensation can substantially be reduced when redesigning the adsorber casing: the actual casing mass (58.9 kg, cf., Table 1) could be strongly decreased as the casing is part of a first iteration lab-scale prototype. Thus, the thermal mass that is heated due to condensation would be lower, which reduces condensation. In turn, the evaporator power, additionally required due to condensation (cf., Section 3.2), would strongly decrease and a condensation protection heater might not be necessary. Third, the impact of condensation can be greatly reduced when improving insulation of the adsorber casing to the environment. For example, the principle of a vacuum flask could be used if the thermal mass of the adsorber casing (i.e., inner flask) is reduced simultaneously. Thus, the temperature of the inner flask would stay almost constant, and a condensation protection heater would not be required. Fourth, we measured steady-state heat losses of the adsorber according to the operating conditions investigated (cf., Section 2.5): for this purpose, the temperature of the condensate protection heater was set to $T_{\rm med}$ while the temperature of the adsorber's heat transfer fluid was set to $T_{\rm med}$ and $T_{\rm high}$, respectively. In both cases, heat did not flow from the ambient/casing into the adsorber heat exchanger (cf., Section 3.2). Instead, the measurements show slight heat losses of the adsorber heat exchanger to the ambient/casing, caused by the fact that the temperature of the adsorber casing was slightly below $T_{\rm med}$ (cf., Section 3.2). These measurements thus show that no heat flows from the condensation protection heater into the adsorber heat exchanger such that this contribution does not need to be considered. In summary, the condensate protection heater only keeps the temperature of the adsorber casing constant, which would not be necessary with a proper design of the adsorber casing according to the recommendations given above.

21944296, 2022, 7, Downloaded from https://onlinelibrary.wiley.com/doi/10.1002/ente.202200251 by Forschungszentrum

Jülich GmbH Research Center, Wiley Online Library on [11/11/2022]. See the Terms

and Conditions (https://onlinelibrary.wiley.com/terms-and-conditions) on Wiley Online Library for rules of use; OA articles are governed by the applicable Creative Commons License

For calculating the heat flows Q_i , steady-state energy balances were applied to the circuits of the heat transfer fluids for each heat exchanger

$$\dot{Q}_i = \Delta \dot{H}_i = \rho_i(T_{i, \text{in}}) \dot{V}_i(h_{i, \text{in}}(T_{i, \text{in}}) - h_{i, \text{out}}(T_{i, \text{out}}))$$
 (3)

where $\Delta \dot{H}_i$ describes the differences in the enthalpy streams of the heat transfer fluids between the inlets and outlets of the heat exchangers; ρ_i/\dot{V}_i are the densities/volume flows of the heat transfer fluids at the heat exchanger inlets; $h_{i,in}/h_{i,out}$ are the specific enthalpies of the heat transfer fluids at the heat exchanger inlets/outlets; $T_{i,in}/T_{i,out}$ are the corresponding temperatures; and i defines the heat exchangers condenser (cond), evaporator (evap), and adsorber (ads). Note that the heat flow during the use phase Q_{use} is only considered when the adsorber outlet temperature $T_{\rm ads,out}$ is greater than the high temperature T_{high} . In the same way, the heat flow during the desorption phase Q_{des} is only considered when the adsorber outlet temperature $T_{\rm ads,out}$ is below the medium temperature $T_{\rm med}$.

Fluid properties of the adsorptive and heat transfer fluids (i.e., water) were calculated using RefProp, [35] with the equation of state from Wagner and Pruß. [36] Measurement uncertainties were carried out according to the "Guide to the Expression of Uncertainty in Measurement" (GUM), [37] with full details given in Section A, Supporting Information.

2.5. Operating Conditions and Control of the AdHT Cycle

A reference case was defined for the operating conditions (Table 3), following the objective of upgrading industrial lowtemperature waste heat to temperatures above 100°C (cf., Section 1). The operating temperatures $T_{\text{low}}/T_{\text{med}}/T_{\text{high}}$ were 25/90/110 °C, corresponding to the use case "constant temperature" (cf., Section 2.1). Accordingly, the temperature of the condensate protection heater $T_{\text{protection}}$ was set to the medium temperature $T_{\rm med}$ to avoid condensation at the inner surface of the adsorber casing. The volume flows $V_{\rm cond}/V_{\rm evap}/V_{\rm use/des}$ were the highest achievable in the respective heat exchangers during the use and desorption phases (i.e., 7/10/8 L min⁻¹), thus ensuring the maximal possible heat transfer for the secondary circuits.

To systematically assess the AdHT performance, we varied the operating conditions for the use case "constant temperature" and compared results with the reference case: the condensate protection heater was deactivated to analyze the impact of condensation at the inner surface of the adsorber casing (measurement set "1," cf., Table 3), and operating volume flows were halved to evaluate heat transfer limitations of the secondary circuits (measurement sets "2-4," cf., Table 3). In addition, the operating temperatures were reduced or increased by 5 K (measurement sets "5-9," cf., Table 3) to analyze the effects of the recooling temperature (i.e., T_{low}), driving temperature (i.e., T_{med}), and useful temperature (i.e., T_{high}). Note that the temperature of the condensate protection heater was always set to the medium temperature T_{med} , and the medium temperature $T_{\rm med}$ was not increased by 5 K due to limitations of the thermostats.

Table 3. Operating conditions of conducted measurement sets: inlet temperature of condensate protection heater of the adsorber (Tprotection); volume flows of heat transfer fluids at inlets of the condenser (V_{cond}) and evaporator (V_{evap}), and at the adsorber inlet during the phases use (\dot{V}_{use}) and desorption (\dot{V}_{des}) ; temperatures of heat transfer fluids at inlets of the condenser (T_{low}) and evaporator $(T_{\rm med})$, and at the adsorber inlet during the phases use $(T_{\rm ads,in})$ and desorption ($T_{\rm med}$); and desired temperature of heat transfer fluid at adsorber outlet during the use phase ($T_{\rm high}/T_{\rm ads,out}$). Values varied compared to the reference case are highlighted in bold.

Variable	$T_{\text{protection}}$	\dot{V}_{cond}	$\dot{V}_{\rm evap}$	\dot{V}_{use}	\dot{V}_{des}	T_{low}	$T_{\rm med}$	$T_{\rm ads,in}$	
Set \ Unit	°C	L min ⁻¹	L min ⁻¹	L min ⁻¹	L min ⁻¹	°C	°C	°C	(i.e., T_{high})
Reference	90	7	10	8	8	25	90	110	>110
1	off	7	10	8	8	25	90	110	>110
2	90	3.5	10	8	8	25	90	110	>110
3	90	7	5	8	8	25	90	110	>110
4	90	7	10	4	4	25	90	110	>110
5	90	7	10	8	8	25	90	105	>105
6	90	7	10	8	8	25	90	115	>115
7	90	7	10	8	8	25	85	110	>110
8	90	7	10	8	8	20	90	110	>110
9	90	7	10	8	8	30	90	110	>110
10	90	7	10	8	8	25	90	100	>100
11	90	7	10	1.3	8	25	90	90	>100

The impacts of the two use cases (cf., Section 2.1) on the AdHT performance were compared at a temperature lift of TL = 10 K, for which the operating temperatures $T_{\text{low}}/T_{\text{med}}/$ $T_{\rm ads,in} \rightarrow T_{\rm ads,out}$ were 25/90/100 \rightarrow > 100 °C and 25/90/ $90 {\rightarrow} > 100\,^{\circ}\text{C}$ (measurement sets "10–11," cf., Table 3). Note that the volume flow of the adsorber was set to the lowest possible value during the use phase (i.e., 1.3 L min⁻¹) for the use case "temperature lift," as the adsorber power was too low to realize the desired temperature lift of 10 K for a greater heat capacity rate.

For each measurement set, we accounted for the trade-off between COP and SHP (cf., Section 2.4) by changing the phase times of the AdHT cycle. The times for the use and desorption phases (τ_{use} and $\tau_{desorption}$) were identical, which is typically for commercial adsorption systems to keep system complexity low, and increased in steps of 100 s starting at 100 s until no useful heat flow Q_{use} was generated in the use phase anymore. The reflux time τ_{reflux} was constant for all measurement sets and set to 30 s, ensuring that all condensed adsorptive was returned into the evaporator. In contrast, the adsorption-based heating and predesorption times (τ_{heating} and $\tau_{\text{predesorption}}$) were controlled in all measurement sets, based on the average adsorbent temperature

$$\overline{T}_{\rm sor} = \frac{T_{\rm sor}^{\rm A} + T_{\rm sor}^{\rm B} + T_{\rm sor}^{\rm C}}{3} \tag{4}$$

The adsorption-based heating ended by automatically switching the corresponding valves once the average adsorbent

21944296, 2022, 7, Downloaded from https://onlinelibrary.wiley.com/doi/10.1002/ente.202200251 by Forschungs/zentrum Jülich GmbH Research Center, Wiley Online Library on [11/11/2022]. See the Terms

on Wiley Online Library for rules of use; OA articles are governed by the applicable Creative Commons License

temperature \overline{T}_{sor} exceeded the high temperature T_{high} by 5 K for at least 5 s. In the same way, the predesorption ended once the average adsorbent temperature $\overline{T}_{\mathrm{sor}}$ was below the medium temperature $T_{\rm med}$ by 5 K for at least 5 s. Note that the minimum times of adsorption-based heating and overall predesorption (i.e., $\tau_{\text{reflux and predesorption}} + \tau_{\text{predesorption}}$) were 22 and 35 s, respectively, due to limitations in the hydraulic circuits when switching between the thermostats for the high and medium temperatures.

Furthermore, we measured the maximum achievable adsorber temperatures as well as the heat losses in condenser, evaporator, and adsorber for each measurement set. For this purpose, an AdHT cycle without useful heat generation was measured using constant phase times (i.e., $\tau_{\text{heating}} = 400 \text{ s}$, $\tau_{\text{reflux and predesorption}} = 60 \text{ s}, \quad \tau_{\text{desorption}} = 500 \text{ s}, \quad \text{and} \quad \tau_{\text{use}} = 0 \text{ s},$ and steady-state heat loss measurements were performed for each heat exchanger separately.

3. Results and Discussions

First, we analyze the AdHT cycle in detail operated according to the reference case (Section 3.1) and derive design rules of AdHTs (Section 3.2). Afterward, we assess the impact of different operating conditions (Section 3.3) and the use cases (Section 3.4) on the AdHT performance.

3.1. Detailed Cycle Analysis of the Reference Case

The AdHT cycle studied shall upgrade heat from below 100 to above 100 °C. To establish the feasibility of this upgrade for our measurement set, we started by measuring the maximum achievable average adsorber temperature \overline{T}_{sor} . The maximum temperature \overline{T}_{sor} is about 127 °C and is reached after 250 s for the reference case (**Figure 3**). The temperature \overline{T}_{sor} increases sharply from 90 to 125 °C in less than 60 s at the beginning of the adsorption-based heating phase. Thus, the AdHT prototype can quickly heat the adsorber from below 100 to above 100 °C by using the heat of adsorption. It should be noted that the temperature \overline{T}_{sor} also decreases sharply from 127 to 93 °C in

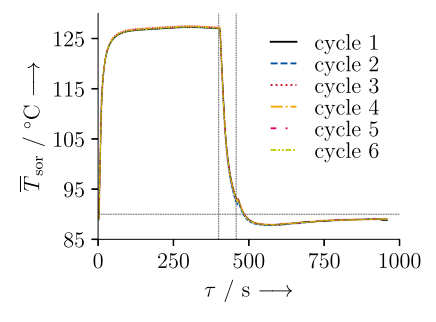


Figure 3. Reproducibility of the maximum achievable average adsorber temperature \overline{T}_{sor} (cf., Equation (4)) for the measurement set "reference" (cf., Table 3). Dashed gray vertical lines indicate phase boundaries (from left to right: adsorption-based heating, predesorption and reflux, desorption; cf., Section 2.5), the dashed gray horizontal line indicates the medium temperature T_{med} , and transparent areas indicate measurement uncertainties (typically within line widths).

less than 60 s at the beginning of the reflux and predesorption phase. Furthermore, the trajectory of the temperature \overline{T}_{sor} is reproduced six times after reaching a cyclic steady-state condition, demonstrating excellent measurement reproducibility within measurement uncertainty. Consequently, we regard the experimental setup designed and built in this work as suitable to measure AdHT cycles.

To increase understanding of the process, we exemplarily analyze trajectories of pressures, temperatures, and differences in enthalpy streams at phase times of 300 s for the use and desorption phases (Figure 4).

Pressure rapidly equalizes at the beginning of the adsorptionbased heating phase and reflux and predesorption phase: the adsorber pressure p_{ads} increases by 475 mbar and drops by 350 mbar in 2 s, respectively (cf., Figure 4a). At the same time,

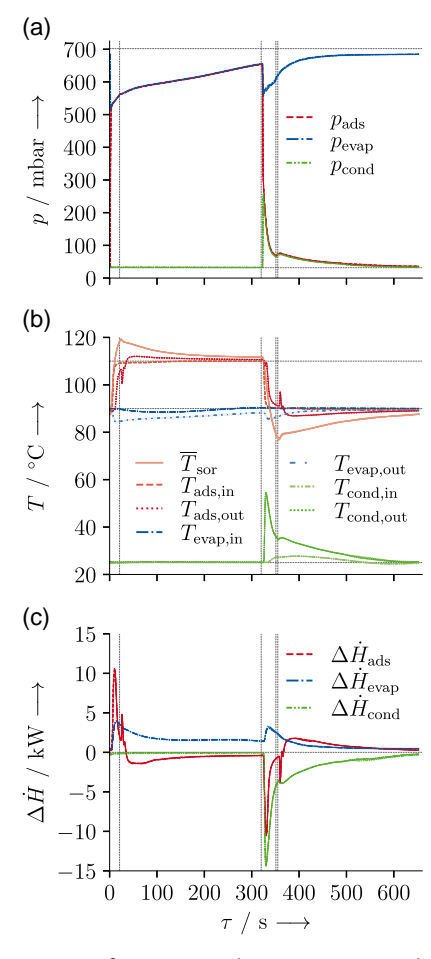


Figure 4. Trajectories of a) pressures, b) temperatures, and c) differences in enthalpy streams in the main components adsorber (ads), evaporator (evap), and condenser (cond) for the measurement set "reference" (cf., Table 3) at phase times $\tau_{\rm use/des} = 300\,\rm s$. All trajectories are reproduced six times at a cyclic steady-state condition. Dashed gray vertical lines indicate phase boundaries (from left to right: adsorption-based heating, use, predesorption and reflux, predesorption, desorption; cf., Figure 1), dashed gray horizontal lines indicate operating temperatures or pressures, and transparent areas indicate measurement uncertainties (typically within line widths).

21944296, 2022, 7, Downloaded from https://onlinelibrary.wiley.com/doi/10.1002/ente.202200251 by Forschungszentrum Jülich GmbH Research Center, Wiley Online Library on [11/11/2022]. See the Terms

of use; OA articles are governed by the applicable Creative Commons I

the evaporator outlet temperature $T_{\rm evap,out}$ decreases from 89.5 to 84 °C (cf., Figure 4b), and the evaporator power $\Delta H_{\rm evap}$ increases from 0.5 to 4 kW (cf., Figure 4c). The condenser outlet temperature $T_{\rm cond,out}$ increases from 25.1 to 54.4 °C (cf., Figure 4b), and the condenser power $\Delta H_{\rm cond}$ increases from 0 to 14.2 kW (cf., Figure 4c). Thus, the rapid pressure equalizations cause fast vaporization and condensation, leading to high mass flow rates of water vapor and high rates of adsorption and desorption. High adsorption and desorption rates induce fast changes in the average adsorbent temperature $\overline{T}_{\rm sor}$ (87.7–118 °C in just 22 s or 111.2 to 77.4 °C in just 35 s, cf., Figure 4b). Consequently, the rapid pressure equalizations cause high system dynamics, which will support the realization of high power densities of the AdHT.

During the use phase, the adsorber pressure p_{ads} slowly increases to 666 mbar (cf., Figure 4a) as the evaporator continuously vaporizes liquid water (cf., Figure 4c). The adsorber pressure increases slowly because the evaporator thermostat limits the evaporator power, as seen by the drop of the evaporator inlet temperature $T_{\text{evap,in}}$ from 90 to 88.5 °C (cf., Figure 4b). Furthermore, the adsorber outlet temperature $T_{ads,out}$ peaks initially (100/107°C, cf., Figure 4b) due to switching the flow direction of the heat transfer fluid from bypass to adsorber (cf., Figure 1b,c). Note that the peak durations agree with 1) the volume flow of the heat transfer fluid $\dot{V}_{use/des}$ and 2) the lengths of the adsorber heat exchanger and its connecting pipes, assuming a plug flow for the incompressible heat transfer fluid. Most importantly, the average adsorbent temperature \overline{T}_{sor} is always higher than the adsorber inlet and outlet temperatures $(T_{\rm ads,in} \text{ and } T_{\rm ads,out})$, and the adsorber outlet temperature $T_{\rm ads,out}$ is always higher than the adsorber inlet temperature $T_{\rm ads,in}$ after 15 s of the start of the use phase (i.e., $\tau_{\text{cycle}} \approx 35$ s, cf., Figure 4b). Thus, the adsorber proved a useful heat flow until the end of the use phase (i.e., $\tau_{\rm cycle} \approx 320 \, \rm s$, cf., Figure 4b), as indicated by the negative adsorber power $\Delta \dot{H}_{ads}$. The same observations are found for the desorption phase; however, the condenser thermostat is less limiting than the evaporator thermostat (cf., Figure 4a, c). Overall, the AdHT cycle is experimentally feasible, successfully using driving heat at 90 °C to generate useful heat above 110 °C.

During the reflux and predesorption phase, pressure rapidly equalizes between the evaporator and reservoir (cf., Figure 4a), resulting in fast vaporization (cf., Figure 4c) and a decrease in the evaporator outlet temperature $T_{\rm evap,out}$ (cf., Figure 4b). In the subsequent predesorption phase, pressure rapidly equalizes between the reservoir and condenser (cf., Figure 4a), causing a slight increase in the condenser power (cf., Figure 4c) and condenser outlet temperature $T_{\rm cond,out}$ (cf., Figure 4b). Consequently, the gravity-supported reflux phase is experimentally feasible. However, it should be noted that the gravity-supported reflux will most likely generate more entropy than pump-supported reflux due to the additional pressure equalizations, resulting in lower AdHT performance.

Overall, the AdHT prototype based on a closed-loop cycle is experimentally feasible for heat transformation from below 100 to above $100\,^{\circ}$ C. Besides, the experimental setup designed in this work shows excellent reproducibility of measurements.

3.2. Deducing Design Rules for Closed-Loop AdHT Cycles

The AdHT performance is evaluated using the efficiency COP and power density SHP (cf., Section 2.4). The trade-off between COP and SHP is accounted for by changing phase times of the use and desorption phase $au_{\mathrm{use/des}}$ (cf., Section 2.5). For the reference case, the highest SHP is 168 W kg-1 and occurs at $COP = 0.178 \, \text{J J}^{-1}$ and phase times $\tau_{\text{use/des}} = 300 \, \text{s}$, while the highest COP is $0.183 \,\mathrm{J}\,\mathrm{J}^{-1}$ and occurs at SHP = $138 \,\mathrm{W}\,\mathrm{kg}^{-1}$ and phase times $\tau_{\rm use/des} = 500 \, \rm s$ (Figure 5). With further increasing the phase times $au_{use/des}$, the COP and SHP would decrease as 1) the negative impact of heat losses becomes predominant and 2) the adsorber outlet temperature $T_{\rm ads,out}$ was already too low at phase times $\tau_{\rm use/des}$ of 500 s to supply useful heat above 110 °C. Overall, the SHP varies stronger than the COP with phase times $au_{\mathrm{use/des}}$ on the Pareto frontier (i.e., results for phase times from 300 to 500 s, cf., Figure 5), which agrees with our findings in a numerical study.[13]

To better assess the observed AdHT performance, we 1) repeat measurements of the AdHT cycle without the condensate protection heater, 2) compensate heat losses, and 3) calculate efficiencies theoretically achievable at maximum. Thereby, three design rules are identified for closed-loop AdHTs.

When turning off the condensate protection heater of the adsorber, the AdHT performance shows the same trends as the reference case (cf., Figure 5). However, the highest power density decreases by about 20% to SHP = 134 W kg⁻¹, and the highest efficiency decreases by about 33% to COP = 0.123 J J⁻¹. Thus, condensation at the inside of the adsorber casing strongly reduces the AdHT performance: more water is vaporized but not adsorbed, thus increasing the required driving heat $Q_{\rm evap}$. The evaporator cannot maintain the same working capacity Δw as in the reference case while condensation is present, decreasing the generation of useful heat $Q_{\rm use}$. Consequently, the first design rule is to avoid condensation inside the adsorber casing to achieve high AdHT performances. Condensation is

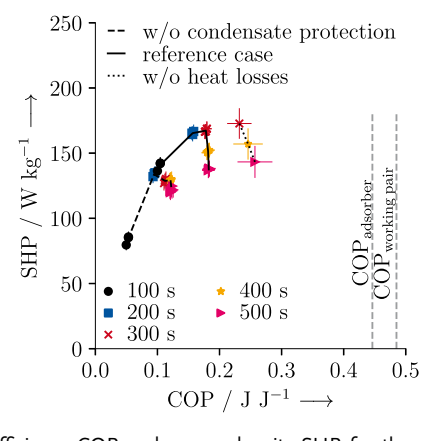


Figure 5. Efficiency COP and power density SHP for the measurement sets "reference" and "1" (cf., Table 3). Phase times of use and desorption phase $\tau_{\rm use/des}$ vary from 100 to 500 s. Dashed gray vertical lines indicate the COP_{working pair} and COP_{adsorber} (cf., Section B, Supporting Information) that are theoretically achievable at maximum. Vertical and horizontal lines at each marker indicate measurement uncertainties (typically within marker sizes).

21944296, 2022, 7, Downloaded from https://onlinelibrary.wiley.com/doi/10.1002/ente.202200251 by Forschungszentrum

Jülich GmbH Research Center, Wiley Online Library on [11/11/2022]. See the Terms and Conditions (https://onlinelibrary.wiley.com/term

on Wiley Online Library for rules of use; OA articles are governed by the applicable Creative Commons License

avoidable, e.g., by redesigning the adsorber. First recommendations for better designs are given in Section 2.4.

Heat losses also reduce the AdHT performance. For the reference case, heat losses measured at steady-state (cf., Section 2.5) are $\Delta \dot{Q}_{\rm evap,loss} = 350 \pm 47 \, \text{W}$ for the evaporator and $\Delta \textit{Q}_{ads,loss} = 22 \pm 42 \, \text{W}$ for the adsorber. Note that the heat losses of the evaporator are higher than those of the adsorber because the adsorber casing is kept constant at the medium temperature T_{med} by a condensate protection heater while the evaporator casing is not (cf., Section 2.2). Compensating for these heat losses shows the strong impact of heat losses on the AdHT performance (cf., Figure 5): the highest efficiency increases by 40% to $COP = 0.257 \text{ J J}^{-1}$; in contrast, the SHP hardly increases as the adsorber has almost no heat losses $\Delta \textit{Q}_{\text{ads,loss}}$ due to the condensate protection heater. Consequently, the second design rule is to ensure sufficient insulation, which is important mainly due to the high driving temperature when recovering industrial waste heat.

To identify the upper limit of measured COPs for the reference case, we calculate theoretical COPs using steady-state equilibrium considerations that indicate maximum achievable efficiencies (cf., Section B, Supporting Information). The Carnot COP is $COP_{Carnot} = 0.807 \text{ J J}^{-1}$, but it considers neither the limitations of the selected working pair nor the selected heat exchanger. When considering the working pair silica gel 123 and water and additionally thermal masses of the adsorber heat exchanger, the maximum achievable efficiency is $COP_{adsorber} = 0.446 \text{ J J}^{-1}$. Thus, the working pair selection and design of the adsorber heat exchanger already reduce the maximum achievable COP by 45%: novel adsorbents with tailor-made equilibrium properties for the selected operating temperatures could increase the maximum achievable COP. Consequently, the third design rule is to select the working pair properly and design the adsorber carefully (i.e., low thermal mass combined with high heat transfer).

Overall, the highest COP of the reference case already achieves 41% of the maximum efficiency $COP_{adsorber}$ achievable for the discussed working pair and adsorber. Besides the quantified heat losses, the AdHT performance is further reduced by 1) nonisothermal use and desorption phases, 2) pressure losses, or 3) the gravity-supported condensate reflux realized by pressure equalizations (cf., Section 2.3). The exact quantification of all losses is beyond the scope of this work and should be addressed in future studies.

3.3. Impacts of Operating Conditions on the AdHT Performance

The operating conditions of the AdHT cycle are varied systematically to explore their impact on the AdHT performance. To check if desired heat transformation is still feasible, we measured the maximum adsorbent temperatures $\bar{T}_{\rm sor,max}$ (Figure 6). Decreasing the medium temperature $T_{\rm med}$ from 90 to 85 °C reduces the temperature $\bar{T}_{\rm sor,max}$ the strongest from 127 to 119 °C. Half of this decrease is found when either halving the volume flows or increasing the low temperature $T_{\rm low}$ from 25 to 30 °C. The reduction of the low temperature $T_{\rm low}$

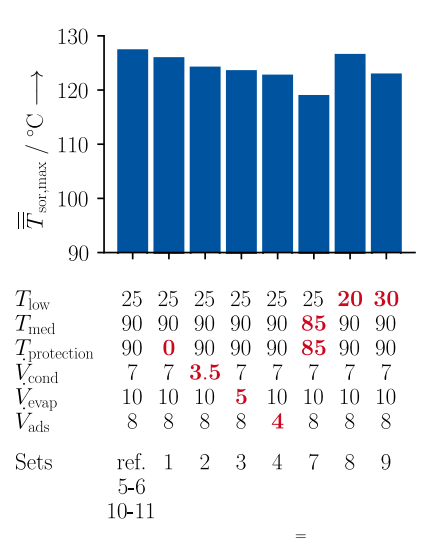


Figure 6. Maximum adsorbent temperatures $T_{\text{sor,max}}$, each averaged over all reproduced cycles, with changed operating conditions (cf., measurement sets defined in Table 3): temperatures T_i are in °C, and volume flows \dot{V}_i are in L min⁻¹. Bold values in red highlight changed operating conditions compared to the reference case.

from 25 to 20 °C hardly changes the temperature $\overline{T}_{sor,max}$ as the working capacity Δw almost stays constant (cf., Section C, Supporting Information). Overall, the heat transformation is feasible from below 100 to above 100 °C for all operating conditions investigated in this work (measurement sets "1–11," cf., Table 3).

Figure 7 shows the impact of volume flows of the heat transfer fluids in the main components on the AdHT performance: the AdHT performance substantially decreases when halving one of the volume flows in the order $\dot{V}_{\rm use/des} > \dot{V}_{\rm evap} \approx \dot{V}_{\rm cond}$.

The decrease in the AdHT performance is almost identical (i.e., within the uncertainty of measurement) when halving

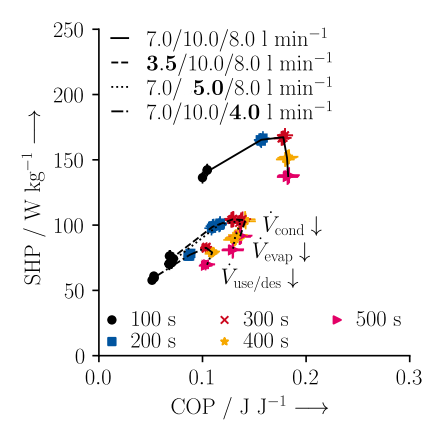


Figure 7. Influence of volume flows $V_{\rm cond}/V_{\rm evap}/V_{\rm use/des}$ on the trade-off between efficiency COP and power density SHP for the operating temperatures $T_{\rm low}=25\,^{\circ}{\rm C}/T_{\rm med}=90\,^{\circ}{\rm C}/T_{\rm high}=110\,^{\circ}{\rm C}$ (measurement sets "reference" and "2–4," cf., Table 3). Varied values are highlighted in bold. Phase times of use and desorption phase $\tau_{\rm use/des}$ vary from 100 to 500 s. Vertical and horizontal lines at each marker indicate measurement uncertainties (typically within marker sizes).

21944296, 2022, 7, Downloaded from https://onlinelibrary.wiley.com/doi/10.1002/ente.202200251 by Forsch

Jülich GmbH Research Center, Wiley Online Library on [11/11/2022]. See the Terms

ditions) on Wiley Online Library for rules of use; OA articles are governed by the applicable Creative Commons

either the condenser volume flow \dot{V}_{cond} from 7 to 3.5 L min⁻¹ or the evaporator volume flow \dot{V}_{evap} from 10 to 5 L min⁻¹. Compared to the reference case, the highest power density decreases by 38% to SHP = 105 W kg⁻¹, and the highest efficiency drops by 23% to COP = 0.141 J J⁻¹. The AdHT performance decreases as a reduction of the volume flows $\dot{V}_{cond}/\dot{V}_{evap}$ limits the heat transfers on the heat transfer fluid's sides: the condenser condenses less of the desorbed water, and the evaporator cannot heat and vaporize the liquid water sufficiently fast. Consequently, the working capacity Δw decreases, reducing the useful heat generation Q_{use} and, in turn, the SHP and COP.

The AdHT performance drops the strongest when halving the adsorber volume flow $\dot{V}_{\rm use/des}$ from 8 to 4 L min⁻¹. The highest power density decreases by 51% to SHP = 83 W kg⁻¹, and the highest efficiency drops by 44% to COP = 0.102 J J ⁻¹. The AdHT performance decreases as the heat transfer limitation during the use phase increases the temperature difference between the adsorbent and heat transfer fluid, thus increasing entropy production and decreasing efficiency. Additionally, the heat transfer limitation during the desorption phase limits regeneration of the adsorbent, thus also reducing the working capacity Δw , the generation of useful heat $Q_{\rm use}$, and the SHP and COP.

Overall, the volume flows should be selected as high as possible when only considering the heat transfer. However, higher volume flows induce higher pressure drops in the main components. Higher pressure drops increase the power consumption of the pumps, which may be relevant in, e.g., exergy or thermoeconomic analyses of an AdHT.

The AdHT performance also depends substantially on the operating temperatures $T_{\rm low}/T_{\rm med}/T_{\rm high}$ (Figure 8).

When reducing the high temperature $T_{\rm high}$ by 5 K to 105 °C, less heat of adsorption is needed to heat the adsorber to the high temperature $T_{\rm high}$ compared to the reference case: the highest power density increases by 43% to SHP = 241 W kg⁻¹, and the highest efficiency increases by 27% to COP = 0.233 J J⁻¹. In contrast, more heat of adsorption is required when increasing the high temperature $T_{\rm high}$ by 5 K to 115 °C: the highest power density and efficiency decrease by 70% and 67% to SHP = 50 W kg⁻¹ and COP = 0.061 J J⁻¹, respectively. Still noteworthy, a temperature lift of 25 K is experimentally feasible at the cost of lower efficiency and power density. Note that the working capacity Δw remaining for the use phase is too small to generate useful heat $Q_{\rm use}$ for longer phase times than $\tau_{\rm use/des}$ = 200 s when increasing the high temperature $T_{\rm high}$.

Reducing the medium temperature $T_{\rm med}$ by 5 K to 85 °C decreases the exploitable working capacity Δw during the adsorption-based heating and use phase compared to the reference case: the highest power density and efficiency decrease by 70% and 60% to SHP = 50 W kg⁻¹ and COP = 0.074 J J⁻¹, respectively. Thus, a sufficiently high medium temperature $T_{\rm med}$ that drives the AdHT is crucial when operating an AdHT, which agrees with our previous numerical analysis. [13] Note that the medium temperature $T_{\rm med}$ was not increased by 5 K due to limitations of the thermostats.

Increasing the low temperature $T_{\rm low}$ by 5 K to 30 °C also reduces the exploitable working capacity Δw during the

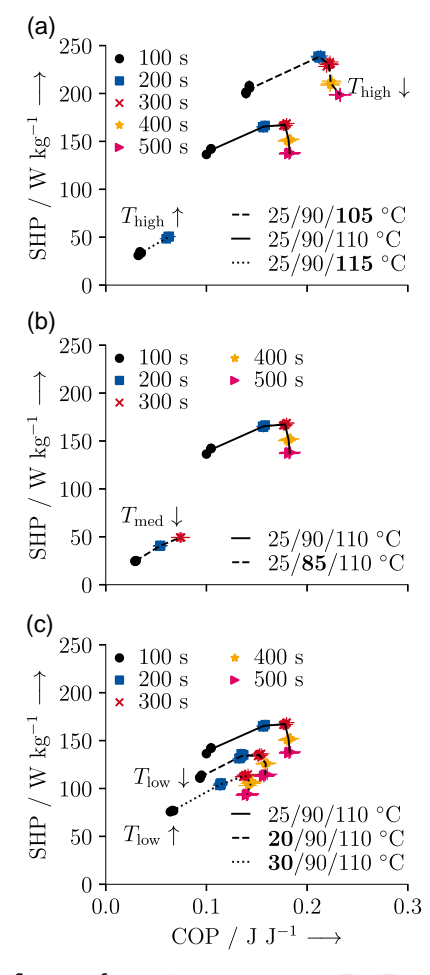


Figure 8. Influence of operating temperatures $T_{\rm low}/T_{\rm med}/T_{\rm high}$ on the trade-off between efficiency COP and power density SHP for the operating volume flows $\dot{V}_{\rm cond}=7$ L min $^{-1}/\dot{V}_{\rm evap}=10$ L min $^{-1}/\dot{V}_{\rm use/des}=8$ L min $^{-1}$ (measurement sets "reference" and "5–9," cf., Table 3). Subfigures show the influence of the a) high-temperature level $T_{\rm high}$, b) medium-temperature level $T_{\rm med}$, and c) low-temperature level $T_{\rm low}$. Varied values are highlighted in bold. Phase times of use and desorption phase $\tau_{\rm use/des}$ vary from 100 to 500 s. Vertical and horizontal lines at each marker indicate measurement uncertainties (typically within marker sizes).

adsorption-based heating and use phase, but less than reducing the medium temperature T_{med} . Thus, the highest power density decreases only by 31% to $SHP = 116 \text{ W kg}^{-1}$, and the highest efficiency decreases only by 21% to $COP = 0.144 \text{ J J}^{-1}$. However, in contrast to our expectations, the AdHT performance drops when decreasing the low temperature T_{low} by 5 K to 20 °C: the highest power density drops by 18% to SHP = 137 W kg⁻¹ and the highest efficiency drops by 13% to $COP = 0.159 \, \text{J}^{-1}$. Although decreasing the low temperature T_{low} increases the working capacity Δw and allows to generate more useful heat Q_{use} , the heat demands for desorption Q_{des} and vaporization Q_{evap} increase simultaneously. Thereby, the heat for vaporization Q_{evap} increases as 1) more water has to be vaporized due to the higher working capacity, and 2) the condensed water has to be heated for a larger temperature thrust $TT = T_{\text{med}} - T_{\text{low}}$. Thus, the AdHT performance shows an optimum value for the low

21944296, 2022, 7, Downloaded from https://onlinelibrary.wiley.

com/doi/10.1002/ente.202200251 by Forschungszentrum Jülich GmbH Research Center, Wiley Online Library on [11/11/2022]. See the Terms and Conditions (https://onlinelibrary.wiley.com/terms

and-conditions) on Wiley Online Library for rules of use; OA articles are governed by the applicable Creative Commons License

temperature T_{low} , discussed in more detail in Section C, Supporting Information.

Overall, the changes in the measured maximum COP qualitatively match the changes in the theoretically maximum achievable COP_{adsorber} when varying the operating temperatures $T_{\rm low}/T_{\rm med}/T_{\rm high}$ (cf., Table S1, Section B, Supporting Information). However, the changes do not match quantitatively, showing that not only the driving force changes but also the exergy efficiency of the process, which is discussed in more detail in Section B, Supporting Information.

3.4. Use Cases "Constant Temperature" versus "Temperature Lift"

As introduced in Section 2.1, an AdHT has two use cases: 1) "constant temperature" and 2) "temperature lift." While the first use case is studied more frequently in the literature, the second use case might be more applicable to industrial processes, as it corresponds to the classic use of a heat pump. Therefore, the "temperature lift" use case is also studied in the following.

The study applies a temperature lift of 10 K (Figure 9). The use case "constant temperature" has the highest power density of SHP = 290 W kg⁻¹ and the highest efficiency of $COP = 0.256 \text{ J J}^{-1}$. For the use case "temperature lift," the highest COP and SHP are slightly lower: the highest power density is $SHP = 280 \text{ W kg}^{-1}$ and occurs almost at the highest efficiency $COP = 0.244 \text{ J J}^{-1}$. The efficiency of the "temperature lift" use case should increase according to the thermodynamic equilibrium model because the thermodynamic mean temperature of the heat transfer fluid in the adsorber decreases slightly (cf., Table S1, Section B, Supporting Information). However, in the "temperature lift" use case, the temperature difference between the adsorbent and heat transfer fluid is larger due to the experimental procedure (i.e., adsorption-based heating

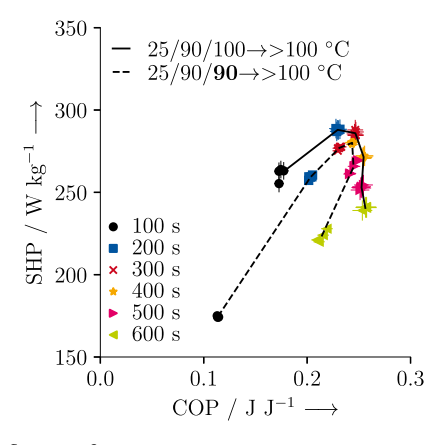


Figure 9. Influence of operating temperatures $T_{low}/T_{med}/T_{ads,in} \rightarrow T_{ads,out}$ on the trade-off between efficiency COP and power density SHP (measurement sets "10-11," cf., Table 3): the solid line indicates the use case "constant temperature" and the dashed line shows the use case "temperature lift." Phase times of use and desorption phase $\tau_{use/des}$ vary from 100 to 600 s. Varied values are highlighted in bold. Vertical and horizontal lines at each marker indicate measurement uncertainties (typically within marker sizes).

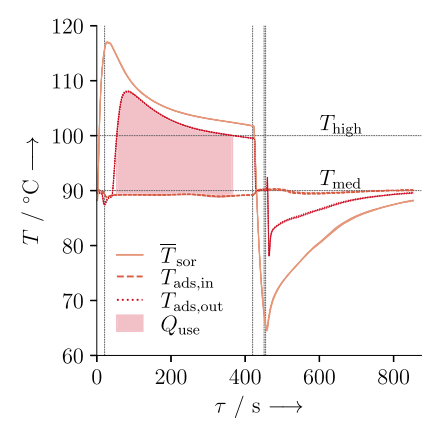


Figure 10. Trajectories of temperatures T in the adsorber (ads) for the measurement set "11" (cf., Table 3) at phase times $\tau_{\rm use/des} = 400 \, \rm s$. All trajectories are reproduced six times at a cyclic steady-state condition. Dashed gray vertical lines indicate phase boundaries (from left to right: adsorption-based heating, use, predesorption and reflux, predesorption, desorption; cf., Figure 1), dashed gray horizontal lines indicate operating temperatures, and transparent areas indicate measurement uncertainties (typically within line widths).

phase, cf., Section 2.5), generating more entropy and decreasing efficiency. In addition, for the "temperature lift" use case, the connecting pipe between the adsorber outlet and the adsorber outlet temperature sensor (i.e., 2.3 kg) must now be heated to the high temperature, also decreasing efficiency. Thus, positive and negative effects seem to balance in practice, resulting in almost equal efficiencies for both use cases.

The use case "temperature lift" achieves the highest SHP at the highest COP due to the definition of the useful heat flow Q_{use} (i.e., zero if $T_{\text{ads,out}} < T_{\text{high}}$, cf., Section 2.4). Once the phase times $au_{\mathrm{use/des}}$ are exceeded at which the adsorber outlet temperature $T_{\rm ads,out}$ reaches the high temperature $T_{\rm high}$ at the end of the use phase (cf., Figure 10), COP and SHP sharply decrease when further increasing phase times $\tau_{\rm use/des}$. This is because useful heat Q_{use} is then no longer generated. However, note that the highest SHP may not occur at the highest COP when selecting lower temperature lifts, at which the nonconstant temperature difference $T_{\rm ads,out}$ – $T_{\rm high}$ is greater than the constant temperature lift $TL = T_{high} - T_{med}$.

Overall, the use case "temperature lift" is experimentally feasible and shows almost the same performance as the use case "constant temperature," thus promising an efficient and flexible integration of an AdHT into industrial processes.

4. Conclusions

The primary energy consumption of the industry can be reduced by transforming low-temperature waste heat from below 100 to above 100 °C. In this work, this heat transformation is experimentally demonstrated for a closed-loop AdHT. For this purpose, we 1) developed an AdHT prototype based on a closed-loop cycle, 2) assessed the power density SHP and efficiency COP for systematically varied operating conditions, and 3) compared the AdHT performance for two use cases to integrate an



AdHT into industrial processes. As a result, four main conclusions can be drawn.

First, the closed-loop AdHT cycle is experimentally feasible at different operating conditions. The lab-scale, one-bed AdHT achieves the highest efficiency COP and power density SHP at 0.183 J J⁻¹ and 168 W kg⁻¹, respectively, for a reference case defined as heat transformation from 90 to 110 °C with the discharge of heat of condensation at 25 °C.

Second, the operating conditions strongly influence the AdHT performance. 1) The volume flows of the heat transfer fluids should be maximized for the highest heat transfer, as the AdHT performance of the investigated prototype drops up to 50% when halved. 2) The temperature lift should be as small as possible and the driving temperature as large as possible to ensure a large working capacity exploitable for adsorption-based heating and generation of useful heat. 3) The condensation temperature has an optimum intermediate value in this work

Third, three design rules are identified for achieving high AdHT performances. 1) Proper adsorber design increases the AdHT performance up to 33% by avoiding condensation at the inside of the adsorber casing. First recommendations for a proper design are given in Section 2.4. 2) Using proper equipment design and insulation reduces heat losses and increases the AdHT performance by up to 40%. 3) Proper working pair selection and adsorber design can substantially increase the maximum achievable efficiency compared to the Carnot efficiency.

Fourth, the use case "temperature lift," where the temperature of the heat transfer fluid is increased as it flows through the adsorber, achieves nearly the same AdHT performance as the use case "constant temperature," where useful heat is released nearly isothermally.

Supporting Information

Supporting Information is available from the Wiley Online Library or from the author.

Acknowledgements

This study was funded by Excellence Initiative of the German Federal and State Governments (number StUpPD_284-17).

Open Access funding enabled and organized by Projekt DEAL.

Conflict of Interest

The authors declare no conflict of interest.

Data Availability Statement

The data that support the findings of this study are available in the supplementary material of this article.

Keywords

low-temperature waste heat utilization, prototype testing, thermal heat

www.entechnol.de

21944296, 2022, 7, Downloaded from https://onlinelibrary.wiley.com/doi/10.1002/ente.202200251 by Forschungs/zentrum Jülich GmbH Research Center, Wiley Online Library on [11/11/2022]. See the Terms

ditions) on Wiley Online Library for rules of use; OA articles are governed by the applicable Creative Commons I

Received: March 15, 2022 Revised: April 13, 2022 Published online: May 6, 2022

- [1] International Institute for Applied Systems Analysis (IIASA), TW12050 - The World in 2050: Transformations to Achieve the Sustainable Development Goals, www.twi2050.org, (accessed: December, 2021).
- [2] I. D. Sachs, G. Schmidt-Traub, M. Mazzucato, D. Messner, N. Nakicenovic, I. Rockström, Nat. Sustain, 2019, 2, 805.
- [3] S. Fawzy, A. I. Osman, J. Doran, D. W. Rooney, Environ. Chem. Lett. 2020, 129, 1339.
- [4] Z. Y. Xu, R. Z. Wang, C. Yang, Energy 2019, 176, 1037.
- [5] a) C. Forman, I. K. Muritala, R. Pardemann, B. Meyer, Renew. Sust. Energ. Rev. 2016, 57, 1568. b) A. Firth, B. Zhang, A. Yang, Appl. Energy 2019, 235, 1314.
- [6] G. Kosmadakis, Appl. Therm. Eng. 2019, 156, 287.
- [7] T. Naegler, S. Simon, M. Klein, H. C. Gils, Int. J. Energy Res. 2015, 39,
- [8] M. Rehfeldt, T. Fleiter, F. Toro, Energy Effic. 2018, 11, 1057
- [9] Y. Q. Yu, P. ZHANG, J. Y. Wu, R. Z. Wang, Renew. Sust. Energy Rev. 2008, 12, 1302.
- [10] a) W. Rivera, R. Best, M. J. Cardoso, R. J. Romero, Appl. Therm. Eng. 2015, 91, 654. b) Z. Xu, R. Wang, Front. Energy 2017, 11, 414.
- [11] I. Chandra, V. S. Patwardhan, Heat Recov. Syst. CHP 1990, 10. 527.
- [12] Y. I. Aristov, Energy 2021, 236, 121892.
- [13] M. Engelpracht, A. Gibelhaus, J. Seiler, S. Graf, N. Nasruddin, A. Bardow, Energy Technol. 2021, 9, 2000643.
- [14] A. Frazzica, V. Palomba, B. Dawoud, Appl. Sci. 2021, 11,
- [15] P. Boruta, T. Bujok, Ł. Mika, K. Sztekler, Energies 2021, 14, 4707.
- [16] P. Goyal, P. Baredar, A. Mittal, A. R. Siddiqui, Renew. Sust. Energ. Rev. 2016, 53, 1389.
- [17] E. Oktariani, A. Noda, K. Nakashima, K. Tahara, B. Xue, K. Nakaso, J. Fukai, Int. J. Energy Res. 2012, 36, 1077.
- [18] B. Xue, Y. Iwama, Y. Tanaka, K. Nakashima, A. T. Wijayanta, K. Nakaso, J. Fukai, Exp. Therm. Fluid Sci. 2013, 46, 54.
- [19] B. Xue, X. Meng, X. Wei, K. Nakaso, J. Fukai, Appl. Therm. Eng. 2015, 88, 451.
- [20] B. Xue, S. Ye, L. Zhang, X. Wei, K. Nakaso, J. Fukai, Energy Convers. Manag. 2019, 186, 93.
- [21] L. Zhang, S. Ye, B. Xue, X. Wei, K. Nakaso, J. Fukai, Int. J. Energy Res. 2020, 44, 5634.
- [22] S. Ye, B. Xue, X. Meng, X. Wei, K. Nakaso, J. Fukai, Sustain. Cities Soc. **2020**, 52, 101808.
- [23] Y. I. Aristov, Int. J. Refrig. 2019, 105, 19.
- [24] a) L. G. Gordeeva, Y. I. Aristov, Energy 2019, 167, 440; b) I. Girnik, M. Tokarev, Y. Aristov, Entropy 2020, 22, 808; c) I. Girnik, A. Grekova, L. Gordeeva, Y. Aristov, Fibers 2020, 8, 51.
- [25] Y. I. Aristov, Appl. Therm. Eng. 2017, 124, 1189.
- [26] I. S. Girnik, Y. I. Aristov, Appl. Therm. Eng. 2019, 146, 608.
- [27] L. G. Gordeeva, M. M. Tokarev, Y. I. Aristov, Theor. Found. Chem. Eng. 2018, 52, 195.
- [28] a) M. M. Tokarev, L. G. Gordeeva, A. D. Grekova, Y. I. Aristov, Appl. Energy 2018, 211, 136; b) M. M. Tokarev, L. G. Gordeeva, A. I. Shkatulov, Y. I. Aristov, Energy Convers. Manag. 2018, 159, 213,
- [29] Tokarev, Energies 2019, 12, 4037.

www.advancedsciencenews.com

www.entechnol.de

- [30] F. Ziegler, Int. J. Therm. Sci. 1999, 38, 191.
- [31] Y. I. Aristov, Appl. Therm. Eng. 2017, 124, 521.
- [32] J. Seiler, PhD Thesis, RWTH Aachen University, 2021.
- [33] F. Lanzerath, J. Seiler, M. Erdogan, H. Schreiber, M. Steinhilber, A. Bardow, Appl. Therm. Eng. 2016, 102, 513.
- [34] H. Rottländer, W. Umrath, G. Voss, Fundamentals of Leak Detection, Leybold GmbH, Cologne, https://www.leyboldproducts.com/media/ pdf/90/c7/87/Fundamentals_of_Leak_Detection_EN.pdf, (accessed: January, 2022).
- [35] E. W. Lemmon, I. H. Bell, M. L. Huber, M. O. McLinden, Reference Fluid Thermodynamic And Transport Properties-REFPROP, Version 10.0, NIST Standard Reference Database 23, National Institute of Standards and Technology, Gaithersburg 2018.
- [36] W. Wagner, A. Pruß, J. Phys. Chem. Ref. Data 2002, 31, 387.
- [37] JCGM, 100:2008: Evaluation of Measurement Data Guide to the Expression of Uncertainty in Measurement, https://www.bipm.org/ utils/common/documents/jcgm/JCGM_100_2008_E.pdf, (accessed: January, 2022).

Energy Technol. 2022, 10, 2200251